


Joint deconvolution of building and downhole seismic recordings: an application to three test cases

Bojana Petrovic⁵  · Stefano Parolai¹ · Giovanna Pianese² ·
S. Umit Dikmen³ · Bolot Moldobekov⁴ · Sagynbek Orunbaev⁴ ·
Roberto Paolucci²

Received: 19 February 2017 / Accepted: 15 August 2017 / Published online: 1 September 2017
© Springer Science+Business Media B.V. 2017

Abstract In this study, the joint deconvolution is applied to recordings of three test cases located in the cities of Bishkek, Kyrgyzstan, Istanbul, Turkey, and Mexico City, Mexico. Each test case consists of a building equipped with sensors and a nearby borehole installation in order to investigate different cases of coupling (impedance contrasts) between the building and the soil by analyzing the wave propagation through the building-soil-layers, and hence resolving the soil–structure-interactions. The three installations considering different dynamic characteristics of buildings and soil, and thus, different building-soil couplings, are investigated. The seismic input (i.e., the part of the wave field containing only the up-going waves after removing all down-going waves) and the part of the wave field that is associated with the waves radiated back from the building are separated by using the constrained deconvolution. The energy being radiated back from the building to the soil has been estimated for the three test cases. The values obtained show that even at great depths (and therefore distances), the amount of wave field radiated back by the building to the soil is significant (e.g., for the Bishkek case, at 145 m depth, 10% of the estimated real input energy is expected to be emitted back from the building; for Istanbul at 50 m depth, the value is also 10–15% of the estimated real input energy while for Mexico City at 45 m depth, it is 25–65% of the estimated real input energy). Such results confirm the active role of buildings in shaping the wave field.

✉ Bojana Petrovic
petrovic@gfz-potsdam.de; petrovic@posteo.de

¹ Centre for Early Warning, Helmholtz Centre Potsdam, GFZ German Research Centre for Geosciences, Helmholtzstraße 7, 14467 Potsdam, Germany

² Department of Civil and Environmental Engineering, Politecnico di Milano, Milan, Italy

³ Earthquake Engineering Department, Kandilli Observatory and Earthquake Research Institute, Bogazici University, Istanbul, Turkey

⁴ Central Asian Institute for Applied Geosciences, Bishkek, Kyrgyzstan

⁵ Helmholtz Centre Potsdam, GFZ - German Research Centre for Geosciences, Helmholtzstr. 7, 14467 Potsdam, Germany

Keywords Dynamic soil–structure interaction · Wave propagation in building–soil structures · Energy back-radiation · Instrumented buildings and downholes

1 Introduction

Studying the dynamic characteristics of civil engineering structures and the soil, and how earthquake-induced shakings influences each other, known as the dynamic soil–structure interaction (SSI), has been a subject of interest within the engineering and seismological communities (e.g., Wirgin and Bard 1996; Bard et al. 1996) since several decades. When the interaction is not limited to individual buildings and the underlying soil, but extended to the seismic interaction of an entire city with the soft soil layers during seismic events, it is called site-city interaction (SCI, e.g., Guéguen et al. 2002; Kham et al. 2006).

In the past, while SSI effects on buildings' dynamic behavior have been studied extensively, the modification of the seismic wave field in superficial soil layers induced by the vibration of surface structures have until now received only limited attention. Nevertheless, it is well known that SSI and SCI in densely urbanized areas may cause non-negligible modifications to ground motions compared with those recorded in the free-field.

The influence of surface structures on seismic wave propagation and the waves generated by structural vibrations in response to seismic ground motions recorded even at large distances in urban areas have been observed by experimental studies for several decades. Jennings (1970) performed one of the first studies in which waves generated by the forced vibration of the Millikan Library were registered at up to 10 km distance. It was followed by a study on the effects of high-rise buildings in Los Angeles excited by shock waves induced by the re-entry of the Columbia space shuttle into atmosphere by Kanamori et al. (1991). Guéguen et al. (2000) analyzed in the Volvi experiment the wave field radiated by a reduced-scale vibrating structure in the Volvi EuroSeisTEst site. Considering two close-by structures, Kitada et al. (1999) analyzed experimentally how structure-soil-structure interactions change the dynamic response of the structures themselves. Chavez-Garcia and Cardenas-Soto (2002) studied the influence of neighboring structures on free-field ground motion by using the H/V spectral ratio. Chazelas et al. (2001) investigated the interaction between structures through the soil by a reduced scale centrifuge experiment.

Primarily, 2D and 3D numerical studies have been performed to analyze the effects of the presence of many high-rise buildings on free-field ground motion and hence, the SSI effects in urban areas, e.g., Wirgin and Bard (1996) and Bard et al. (1996). Moreover, several 2D and 3D numerical simulations of ground motions have been carried out in order to investigate the SCI (e.g., Guéguen et al. 2002; Semblat et al. 2002, 2004, 2008; Kham et al. 2006). Different numerical studies have suggested both increases and decreases in ground motion due to buildings located at the Earth's surface. For example, Guéguen et al. (2002) carried out numerical simulations to analyze the contribution of the Roma Norte district of Mexico City to total seismic ground motion. They stated that modifications to the seismic wave field (compared to the free-field case) due to surface structures that behave as secondary seismic sources and local interactions between structures through the soil might be significant in urban areas and defined these effects of a city to the soil as SCI. Kham et al. (2006) analyzed the multiple interactions between soil layers and built structures in dense urban areas, and hence, the influence of the city on the ground motion using simplified 2D boundary elements models. Pioneering examples of more advanced numerical approaches, where a comprehensive 3D modeling of both soils and built

structures in an urban environment is considered, were recently illustrated by Mazzieri et al. (2013) and Isbilibiroglu et al. (2015).

Moreover, several authors have attempted to give a semi-analytical description of the SCI effects. Guéguen et al. (2000) tried to describe the effects of a city by adding the single contribution of each building represented by a single oscillator. Boutin and Roussillon (2004) described the multiple interactions of buildings through homogenization methods.

Studies combining both experimental tests and numerical simulations have been carried out. Bard et al. (2008) observed structure-soil-structure effects by centrifuge tests and numerical simulations. Ditommaso et al. (2009) analyzed the influence of a single vibrating building on the free-field ground motion, while Guéguen and Colombi (2016) investigated the clustering effects of structures on their response.

The deconvolution approach (Kanai 1965), following Snieder and Safak (2006) has found a wide application for studying wave propagation in buildings (e.g., Picozzi et al. 2009; Newton and Snieder 2012; Rahmani and Todorovska 2013; Nakata and Snieder 2014; Cheng et al. 2015; Petrovic et al. 2017) using both ambient vibration measurements and earthquake recordings. Moreover, when applied to downhole strong-motion data, information about the wave propagation in shallow geological layers is obtained (e.g., Mehta et al. 2007a, b; Parolai et al. 2009, 2013; Oth et al. 2011; Raub et al. 2016).

Recent studies have shown the importance of the interactions between objects located at the surface (trees or buildings) in the modification of the seismic wave field. Colombi et al. (2016) performed experimental studies and finite element simulations to better understand the interaction between trees and the soil. Petrovic and Parolai (2016) proposed a method to study the wave propagation in building-soil layers by joint deconvolution and to estimate the wave field being radiated back from a building to the soil.

In this study, we investigated three different cases of coupling (impedance contrast) between the building and the soil by analyzing the wave propagation through building-soil-layers, and thus the soil–structure interaction effects. The objective of this study was to determine the energy radiated back to the subsoil from a building under seismic excitation. For this purpose, the joint deconvolution (Petrovic and Parolai 2016) is applied to earthquake recordings of three installations composed of a borehole and a nearby building equipped with sensors (in the cities of Bishkek, Kyrgyzstan, Istanbul, Turkey, and Mexico City, Mexico). The three test cases involve different soil conditions and building construction types. The ratio between the shear wave velocities of building and soil vary from test site to test site (Bishkek: $v_{\text{soil}} > v_{\text{building}}$, Istanbul: $v_{\text{soil}} \approx v_{\text{building}}$ and Mexico City $v_{\text{soil}} \approx /<v_{\text{building}}$), leading to different impedance contrasts. The shear wave velocity profiles of the soil were provided by previous studies (Parolai et al. 2012, 2013; Meli et al. 1998), while the shear wave velocity through the building was estimated by the application of the deconvolution approach. Although we are considering different ratios between buildings and soil, the impedance of the building is always lower than the impedance of the soil, leading to an impedance contrast below 1 for all considered test cases (Bishkek: $c \approx 0.1$, Istanbul: $c \approx 0.2\text{--}0.3$, Mexico City: $c \approx 0.3\text{--}0.6$). This is due to the fact that the effective density of buildings is always several times smaller than the density of the soil. The seismic input (i.e., the part of the wave field containing only the up-going waves after removing all down-going waves) and the wave field that is associated with the wave field radiated back from the building to the soil is reconstructed using the constrained deconvolution approach. Finally, the energy being radiated back from the buildings to different soil depths is estimated. The influence of different impedance contrasts on the wave field radiated back from the building to the soil is also investigated.

2 Methodology

A two stage approach proposed by Petrovic and Parolai (2016) is used to determine the energy radiated back by the building to subsoil. In the first stage, the joint deconvolution of recordings from the building and downhole sensors is carried out. Then in the second stage, the energy radiated back from the building to the shallow geological layers is estimated. In the following, the main steps of the procedure (Fig. 1) are briefly summarized.

1. Joint deconvolution of building and downhole recordings

The joint deconvolution is an upgrade of the deconvolution approach that has found wide application in the past when applied separately to recordings from buildings or downhole, making it possible to study the wave propagation either through the building or the shallow geological layers, respectively. In our case, the recordings of sensors installed in a building and a borehole are analyzed jointly.

The ground motion recordings at a generic location (within the building or the borehole) are deconvolved by the recording at a reference station (usually either the top or the bottom sensor of a building-downhole-installation) as follows

$$S(\omega) = \frac{u(z_1, \omega)}{u(z_2, \omega)} \quad (1)$$

with $u(z_1, \omega)$ and $u(z_2, \omega)$ being the Fourier transforms of the recordings at depths z_1 and z_2 , respectively. Since this problem is ill-conditioned, to avoid the potential instabilities in the inversion, a regularized Tikhonov deconvolution $S_\varepsilon(\omega)$, defined as

$$S_\varepsilon(\omega) = W_\varepsilon(\omega) \frac{u(z_1, \omega)}{u(z_2, \omega)}, \quad (2)$$

is used (Tikhonov and Arsenin 1977; Bertero and Boccacci 1998). $u(z_1, \omega)$ and $u(z_2, \omega)$ are the Fourier transforms of the recordings at depths z_1 and z_2 and the filter $W_\varepsilon(\omega)$ is given as

$$W_\varepsilon(\omega) = \frac{|u(z_2, \omega)|^2}{|u(z_2, \omega)|^2 + \varepsilon}. \quad (3)$$

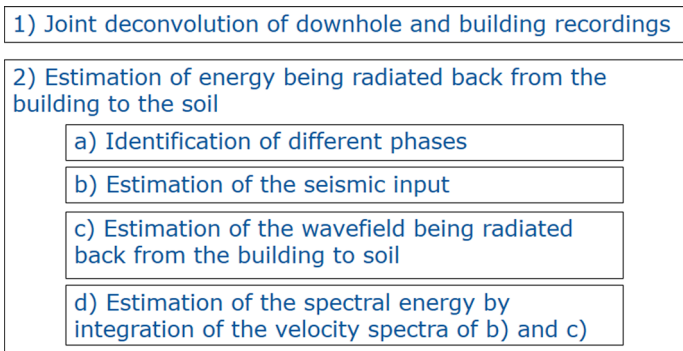


Fig. 1 The general scheme of the methodology followed in this work

where ε is the regularization parameter that is defined as a percentage of the average spectral power. It is a positive constant added to the denominator to prevent the numerical instability of $S(\omega)$. For $\varepsilon = 0$, Eq. (2) is equal to Eq. (1).

In this study, the horizontal components of ground motion are considered, which are expected to be mainly related to the S-wave propagation (e.g., Mehta et al. 2007a, b; Parolai et al. 2009). Before the application of the joint deconvolution, the data are first cosine-tapered at both ends and then, band-pass Butterworth filtered (Bishkek: 1–10 Hz, Istanbul: 0.1–15 Hz, Mexico City: 0.1–5 Hz). The sensor at the top of the building is used as the reference station for the joint deconvolution. The regularization parameter was set to $\varepsilon = 10\%$ of the average spectral power for Bishkek and $\varepsilon = 5\%$ of the average spectral power for Istanbul and Mexico City after trial and error tests (e.g., Bindi et al. 2015).

2. Estimation of the energy being radiated back from the building to the soil

The method for the estimation of the energy being radiated back from the building to the soil consists of four steps.

- a. Identification of the peaks in the deconvolved wave field related to the different phases (upward propagating waves, downward propagating waves reflected at the Earth's surface, at impedance contrasts and at the top of the building, etc.).
- b. Reconstruction of the seismic input at a certain depth related only to the upward propagating waves and hence, by removing all downward propagating waves (reflected at the building's roof, the Earth's surface and the impedance contrasts) using an approach similar to the one proposed by Bindi et al. (2010), based on a constrained regularized scheme (projected Landweber method).

The seismic input is obtained by convolving the peaks related to the upward propagating waves in the deconvolved wave field (using the recordings of the surface downhole sensor as reference) and the recordings at 0 m.

- c. Separation of the part of the wave field that is associated with the waves being radiated back from the building to the soil down to different depths using the same approach as the one used to reconstruct the seismic input (b). Differently from (b), however, the recordings by the roof sensor are used as the reference.

In order to reconstruct the wave field of interest, the peak in the deconvolved wave field, which is associated with the down-going waves being radiated back from the building to the soil, is convolved with the recordings made at the top of the building. Please note that different phases might arrive at the same time and hence overlap (Petrovic and Parolai 2016). For this reason, the relative importance of the contributions of the different phases arriving at the same time has to be taken into account. This is obtained by calculating the analytical transfer functions. Only information on the velocities (obtained from the deconvolution approach) and the densities (mainly of importance for the building's structure, can be estimated) is required. No information on the quality factor Q , which may be complicated to estimate, is needed.

- d. Estimation of spectral energy radiated back from the building to the soil. The spectral energy of the seismic input (b) and the downward propagating waves (c) is obtained by the integration of the velocity spectra of (b) and (c) over a defined frequency band (the same as the one used for the joint deconvolution). The spectral energy of the waves being radiated back from the building to the soil is given relative to the energy of the seismic input and thus, obtained as the ratio of the spectral energies of (c) to (b).

3 Description of the test sites

In this study, three test cases (Bishkek, Kyrgyzstan; Istanbul, Turkey; and Mexico City, Mexico; Figs. 2, 3, 4, 5) with different soil and building characteristics are investigated. If no information is already available on the shear wave velocity profiles of the building and/or the soil, the shear wave velocity can be determined from the deconvolved wave fields. In this study, the shear wave velocity profiles of the soil are provided by previous studies and have been confirmed by the deconvolution approach, while for the buildings these are estimated by the deconvolution approach. After the deconvolution, the deconvolved wave fields are obtained by applying the inverse Fourier Transform. Then, the time lags between

Fig. 2 Installations in CAIAG (green squares) and the adjacent borehole (blue triangles) of the Bishkek test site, showing an image of the CAIAG building (top), the shear wave velocity profile obtained from inverting of the spectra of the deconvolved wave field and the stratigraphy (modified after Parolai et al. 2013)

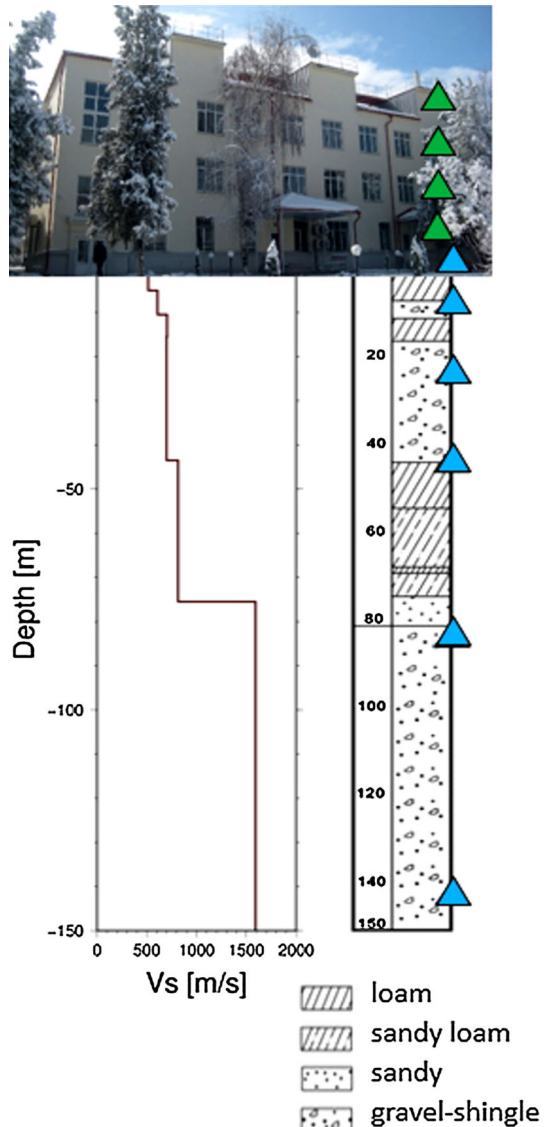
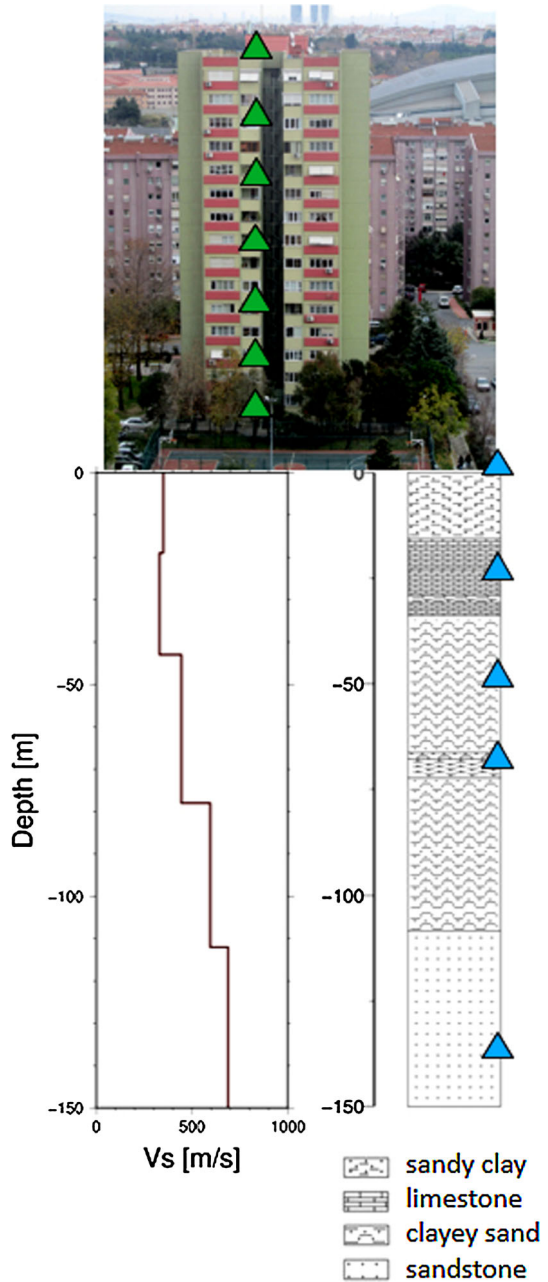


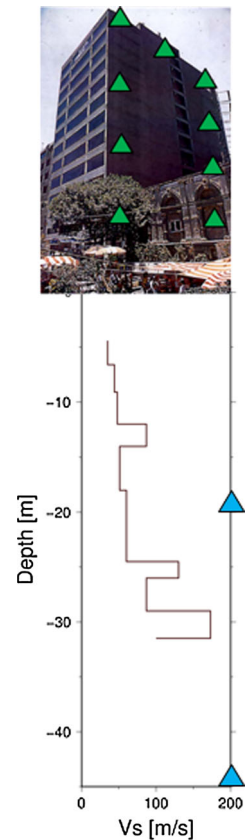
Fig. 3 Installations in building B22 (*green squares*) and the borehole (*blue triangles*) of the Ataköy, Istanbul test site, showing a photo of the building, the shear wave velocity profile obtained from the inversion of the spectra of the deconvolved wave field and the stratigraphy (modified after Parolai et al. 2012)



the upward and downward propagating waves in the deconvolved wave fields and the height differences between the floors where the sensors are installed, are considered. The shear wave velocity is then calculated using a least squares fit.

In Bishkek, the test case is a 3-story reinforced-concrete masonry building with a lower shear wave velocity (~ 300 m/s) than the underlying soil (~ 600 m/s). In Istanbul, the

Fig. 4 Installations in the Jalapa building (*green triangles*) and the borehole (*blue triangles*) of the Mexico City test site, showing an image of the Jalapa building and the shear wave velocity profile obtained from SCT tests (modified after Meli et al. 1998)



shear wave velocity in the uppermost layer (~ 300 m/s) is similar to that through the investigated 16 story tunnel formwork building (distance to downhole installation ~ 50 m). In Mexico City, a 14 story RC building constructed on low velocity clay soil has a similar/higher shear wave propagation velocity (70–140 m/s) to than the subsurface (~ 70 m/s). Nevertheless, it is worth mentioning that the higher density contrast (compared to the velocity contrast) of the buildings and the soil has a major influence on the impedance contrast and hence, on the proportion of the wave field being radiated back from the building to the soil. Additional details of each site are given below.

3.1 Bishkek, Kyrgyzstan

A 150 m deep borehole was drilled in 2010 in Bishkek (Kyrgyzstan) in the courtyard of Central Asia Institute for Applied Geosciences (CAIAG, Fig. 2) and equipped with borehole sensors at 0, 10, 25, 45, 85 and 145 m depth (Parolai et al. 2013; Petrovic and Parolai 2016). Figure 2 shows the S-wave velocity (v_s) structure and the stratigraphy at this site, including the results of the best fitting S-wave velocity models obtained after the inversion of the spectra of the deconvolved wave field (Parolai et al. 2013). Above 80 m depth the soil is composed of alternating layers of coarse gravel shingle and sandy layers of

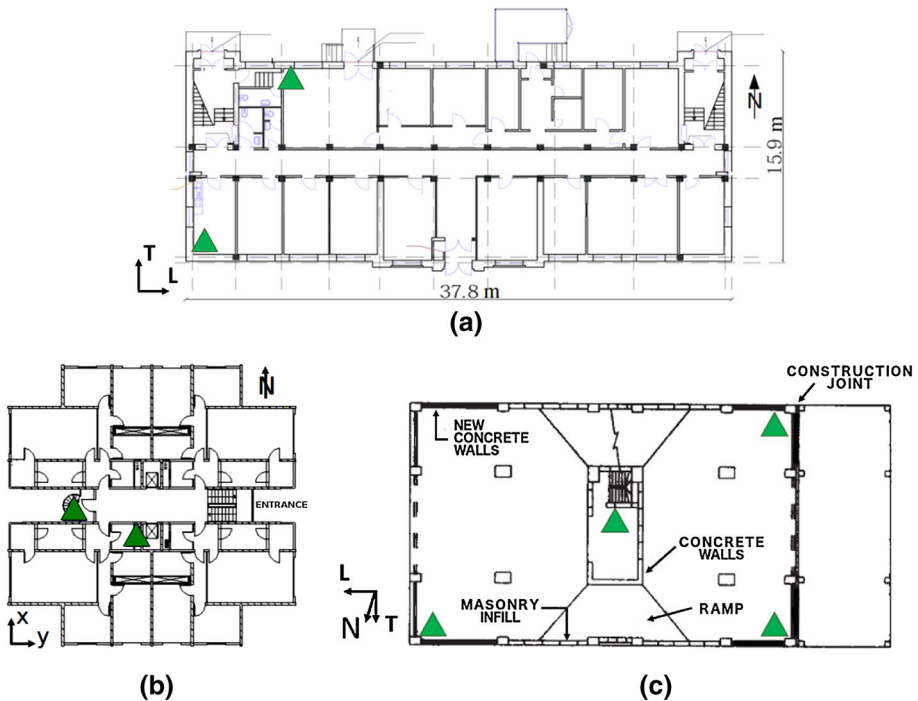


Fig. 5 Footprints of the three investigated buildings (**a** CAIAG institute, Bishkek, Kyrgyzstan, **b** B22 building, Istanbul, Turkey, **c** Jalapa building, Mexico City, Mexico). The location (green triangles) and orientation of the sensors is also shown (modified after Petrovic and Parolai 2016 and Murià-Vila et al. 2001)

different thicknesses, while from 80 to 150 m depth there is a thick gravel-shingle layer. For further information on this borehole installation, see Parolai et al. (2013).

The building of the CAIAG institute (distance to borehole installation ~ 10 m) has been equipped with seven SOSEWIN (Self-Organizing Seismic Early Warning information Network, Fleming et al. 2009) units since 2012, with six at two edges of the three floors and one under the roof (Figs. 2, 5a). The CAIAG building is a three story reinforced masonry structure built in 1975. The footprint (Fig. 5a) of the building is rectangular ($37.8 \text{ m} \times 16.3 \text{ m}$), the walls are constructed of fired clay solid bricks, concrete floors and roof of timber frame with metal cover (Petrovic and Parolai 2016).

3.2 Istanbul, Turkey

In December 2005, in the district of Ataköy, Istanbul (Turkey), four boreholes of 25, 50, 70 and 140 m (Fig. 3) were drilled and equipped with 3 shallow boreholes accelerometers (at 25, 50 and 70 m) and a deep borehole accelerometer (at 140 m depth). In addition, a sensor at 0 m was installed (Parolai et al. 2009, 2010, 2012; Bindi et al. 2010). The sensor at 70 m had experienced some malfunctions during the analyzed time period and hence, its recordings could not be used. Figure 3 shows the S-wave velocity structure and the stratigraphy at the test site. The shear wave velocity profiles has been obtained by inversion of the spectra of the deconvolved wave fields, the best-fitting v_s model is shown in Fig. 3

(Parolai et al. 2012). In this part of the city, alluvial deposits (unconsolidated sediments composed of gravel, sand, silt and clay) overlie the Bakirköy and Güngören formations over Palaeozoic bedrock (Sorensen et al. 2006). A detailed description of the borehole installation is given in Parolai et al. (2009).

A 16 story (including one basement story) tunnel formwork building (B22), located ~ 50 m from the borehole, has been equipped by a SOSEWIN network consisting of 15 stations (four of them connected to 5TC Güralp strong motion accelerometers) installed near to the building's center and the fire escape staircase (Fig. 5b) at different floors since September 2015. The first SOSEWIN installation, consisting of only three SOSEWIN stations placed at the basement, the 8th floor and the roof, was realized in the summer of 2013. The building was constructed in the early 1990s, and has a total height of about 45 m and an approximately square footprint with dimensions of 23.1 m × 23.9 m (Fig. 5b). The building is symmetrical in both perpendicular directions in plan view, with four apartments of the same size located at each floor. The exterior walls with windows were constructed using precast panels. The interior walls and the remaining exterior walls, i.e., those without windows are made of reinforced concrete and are 15 and 20 cm thick. For further information on the building's structure and the dynamic characteristics of the building, see Petrovic et al. (2017).

3.3 Mexico City, Mexico

The Jalapa building in Mexico City, Mexico, constructed in 1981, is a 14 story reinforced concrete building (Figs. 4, 5c), located in the central area of the city. The building was instrumented with 11 tridirectional solid state digital accelerographs (Terra Technology DCA-33R) at different locations on 4 floors (basement, 6th and 11th floor, roof, Fig. 4) from 1992 to 2004. The first three stories of the Jalapa building are used as parking, the others as offices. The building is 39.5 m high with a rectangular footprint (19.4 m × 40 m from the basement to the 3rd floor, and 19.4 m × 32.45 m from the 3rd floor to the roof, Fig. 5c). The original structural system is of a waffle flat-plate on rectangular columns, with a small core of concrete shear walls around the shafts for the staircases and elevator, and masonry infill walls in external frames in a longitudinal direction and around the staircases.

The borehole installation consisted of two accelerographs (same instrument type as those installed in the building) at 20 and 45 m depth underneath the basement of the building. Beneath a superficial crust (5 m thick), soft clay deposits (down to 29.5 m depth) overlie a 3 m thick intermediate firm layer. A lower clay layer (from 32.5 to 38.5 m depth) is followed by deep firm deposits. The shear wave velocity profile obtained from SCT tests (Meli et al. 1998) is shown in Fig. 4.

The Jalapa building is one of the few well-instrumented buildings in Mexico that have suffered structural and non-structural damage, and it has been retrofitted twice during its lifetime (Murià-Vila et al. 2001). Thus, it is of great interest for the earthquake engineering community, with the dynamic behavior of the building being studied in detail, e.g., by Meli et al. (1998) and Murià-Vila et al. (2001). Moreover, due to its location on a very soft clay soil, soil–structure interaction effects have also been observed (e.g., Paolucci 1993; Faccioli et al. 1996; Cardenas et al. 2000; Murià-Vila et al. 2004). A first attempt to analyze the strong motion recorded by the borehole and building installation jointly was made by Cardenas-Soto (2007). Pianese et al. (2017) presented a new methodology for the detection of non-linear response of instrumented buildings during an earthquake by combining

Stockwell Transforms (Stockwell et al. 1996) and the deconvolution approach and applying this to the Jalapa building.

4 Data set

4.1 Bishkek, Kyrgyzstan

The data set used in this study for the Bishkek test case is composed of four earthquake recordings (Table 1; Fig. 6a) with magnitudes ranging from M 4.8 to 5.2, that occurred between November 2013 and March 2015 in Kyrgyzstan or Kazakhstan.

The horizontal components of the borehole sensors are rotated in order to be orientated along the main building axes. The data of the SOSEWIN units is resampled by interpolation (originally 100 samples per second) in order to obtain the same sampling rate as the data from the downhole sensors (500 samples per second) to improve the resolution of the deconvolution results in the time domain (e.g., Céspedes et al. 1995; Tamim and Ghani 2010).

4.2 Istanbul, Turkey

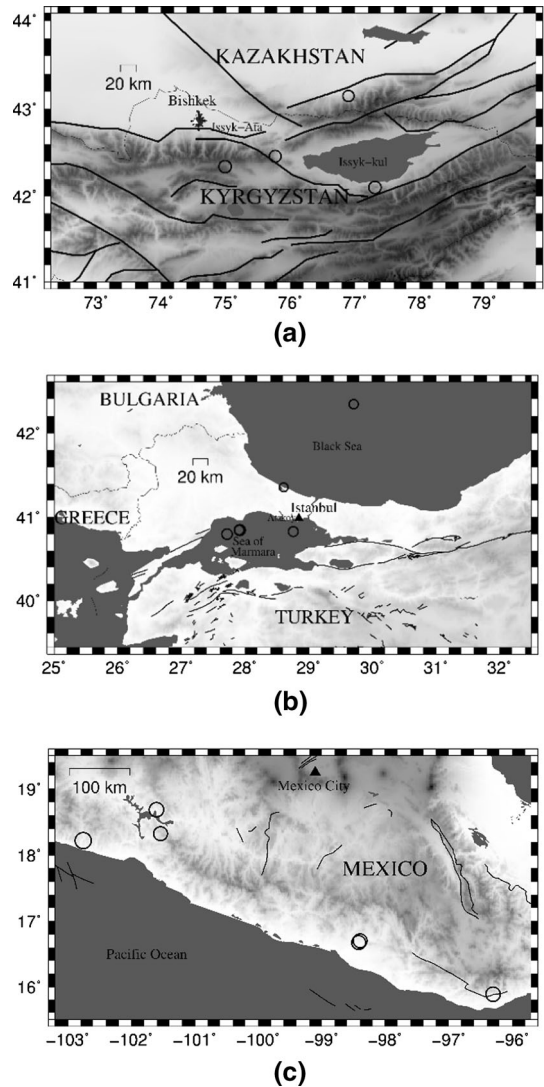
The analyzed data set (Table 2; Fig. 6b) consists of six earthquake recordings with magnitudes between M_w 3.7–4.8 (with epicentral distances from 20 to 165 km) that occurred between November 2013 and December 2015, four of which were in the Marmara Sea region. Earthquakes that were registered at least at the sensor at the building's roof and at the 140 m deep downhole sensor are considered. It is worth mentioning that three of the six events (Table 2, event 1–3) took place before the new dense SOSEWIN installation and hence, for these events only the recordings at the top and the bottom of the building are available. Moreover, since only small events and the corresponding weak motions are used for this study, and due to the lower quality of the MEMS sensors used by the SOSEWIN units, only recordings of 5TC Güralp strong motion accelerometers connected to the SOSEWINs are used.

The data from the sensors installed in the borehole are rotated in such a manner that the two horizontal components are oriented along the main building axes. The data from the SOSEWIN sensors is resampled (original sampling rate 100 samples per second) in order to have the same sampling rate same as of the borehole sensors (200 samples per second).

Table 1 List of events used in this study for the test site in Bishkek, Kyrgyzstan

Event ID	Date	Time (UTC)	Location	Depth (km)	Magnitude (M_w)	Distance to epicenter (km)
BI-2013	23.11.2013	09:42:08	42.46N, 75.77E	10	4.9	110
BI-2014	14.11.2014	01:24:20	42.10N, 77.31E	45	5.2	350
BI-2015-1	22.01.2015	15:52:29	42.34N, 77.99E	0	4.9	280
BI_2015-2	15.03.2015	14:01:02	43.15N, 76.90E	10	4.8	190

Fig. 6 Locations of the epicenters (*circles*) of the earthquakes used in this study for **a** Bishkek (events listed in Table 1), **b** Istanbul (Table 2), and **c** Mexico City (Table 3)



4.3 Mexico City, Mexico

During the installation period, several seismic events were recorded in the Jalapa building. In our study, we focus on those events that did not cause any damage to the building, and hence the building's behavior can be approximated as being linear for the considered events (Meli et al. 1998; Murià-Vila et al. 2001). The characteristics of the 6 analyzed events with magnitudes M_w 6.0–7.2 and epicentral distances of approximately 300–400 km (Fig. 6c) are given in Table 3. Apart from the two other test cases where the buildings were not damaged until now and hence, the dynamical characteristics of the buildings can be assumed to be constant over time, for the Jalapa building, the dynamic properties have been altered due to structural damage and retrofitting.

Table 2 List of events used in this study for the test site in Istanbul, Turkey

Event ID	Date	Time (UTC)	Location	Depth (km)	Magnitude (M_w)	Distance to epicenter (km)
IS-2013-1	27.11.2013	04:13:37	40.85N, 27.92E	9	4.8	80
IS-2013-2	27.11.2013	04:21:35	40.85N, 27.91E	7	4.0	80
IS-2014	05.02.2014	01:56:44	41.36N, 28.61E	12	3.7	45
IS-2015-1	28.10.2015	16:20:03	40.80N, 27.72E	16	4.6	100
IS-2015-2	16.11.2015	15:45:43	40.83N, 28.76E	8	4.3	20
IS-2015-3	15.12.2015	01:13:39	42.34N, 29.71E	30	4.1	165

Table 3 List of events used in this study for the test site in Mexico City, Mexico

Event ID	Date	Time (UTC)	Location	Depth (km)	Magnitude (M_w)	Distance to epicenter (km)
MC-1993-1	15.05.1993	03:09:38	16.67N, 98.42W	19.7	6.0	318
MC-1993-2	15.05.1993	03:12:32	16.70N, 98.40W	20.8	6.1	315
			Damage + retrofitting			
MC-1997-1	11.01.1997	20:28:26	18.22N, 102.0W	33	7.2	330
MC-1997-2	22.05.1997	07:50:53	18.68N, 101.6W	70	6.5	270
MC-1998	03.02.1998	03:02:00	16.67N, 96.42W	33	6.3	515
			Damage			
MC-1999-2	21.06.1999	17:43:04	18.32N, 101.54W	68.7	6.2	285

5 Results—joint deconvolution and estimation of the energy being radiated back from the building to the soil

5.1 Joint deconvolution

The recordings for one horizontal component (Bishkek: transverse component, Istanbul: x-direction, Mexico City: transverse direction, see Fig. 5) of each building-downhole installation and the corresponding Fourier amplitude spectra (FAS) are shown exemplarily for one event for each test site in Figs. 7, 8 and 9 (Fig. 7: Bishkek, event BI-2015-2, M_w 4.8, Table 1; Fig. 8: Istanbul, event IS-2015-1, M_w 4.6, Table 2; Fig. 9: Mexico City, event MC-1993-2, M_w 6.1, Table 3).

For all three test cases, the variation in the ground motion with depth/height and the higher level of shaking in the buildings is observed. When considering the recordings of the sensors installed in the buildings (especially the higher floors and the roof) for the Istanbul and Mexico City installations, the shaking of the building is univocal. The Fourier spectra show clearly the different frequency ranges where most of the energy is concentrated for the building and the downhole sensors for the test cases in Bishkek and Istanbul. The Fourier amplitude spectra of the Mexico City installation show only a small variation in the frequency content with depth due to similar fundamental frequencies (i.e., building: $f_{T1} = 0.44$ Hz, soil: $f_{soil} = 0.5$ Hz) and the frequency content of building and the soil (e.g., Meli et al. 1998). Moreover, the frequency band for the Mexico City case containing most of the energy is much narrower than for the other two test cases, with a frequency range only up to 3 Hz. For Mexico City, most of the energy is located between 0.2 and

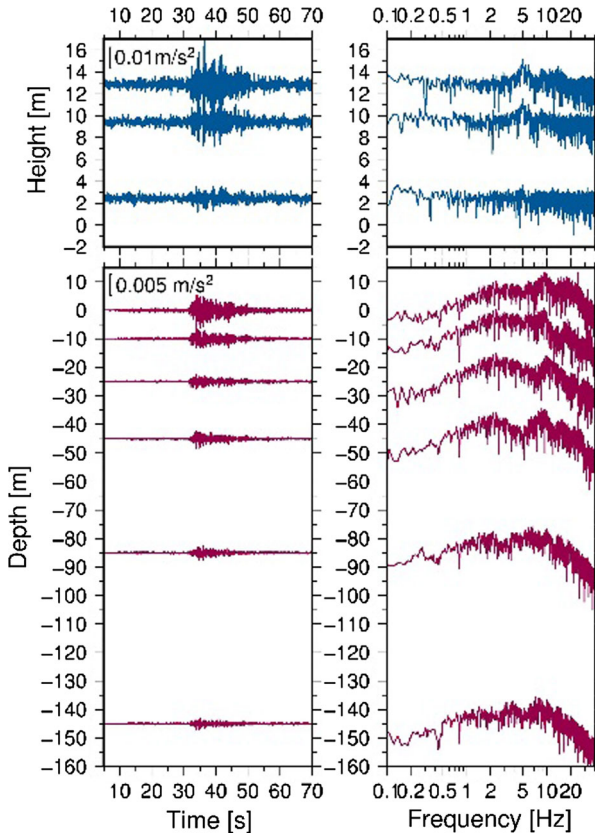


Fig. 7 Recordings of transverse component (*blue lines* building sensors, *magenta lines* downhole sensors) and the corresponding Fourier Spectra for the Bishkek vertical array, event BI-2015-2, Table 1

2 Hz since the thick layers of extremely soft clay act as a band pass filter and greatly amplify the seismic waves coming from deeper firm strata. This results in an almost monochromatic ground motion of long duration and low frequencies (Murià-Vila et al. 2001). For the Bishkek test case, a clear resonant peak is estimated at $f = 5$ Hz in the Fourier spectra of the recording at the roof's station, most likely due to the 1st bending mode in this direction at $f = 5$ Hz (Petrovic and Parolai 2016). For the installation in Istanbul, the Fourier spectra of the building sensors, especially for the higher floors and the roof, are not dominated by only one resonant peak, but by three ($f_1 = 1$ Hz, $f_2 = 3.84$ Hz and $f_3 = 7.5$ Hz), corresponding to the first three bending modes in this direction. Interestingly, for the B22 building, the higher modes (especially the second one) also make a high contribution to the building's dynamic behavior and are clearly visible in the deconvolved wave field, as was shown and discussed in Petrovic et al. (2017). For the Jalapa building, a peak at around 0.4 Hz (corresponding to the first bending mode in the transverse direction) can be assumed in the FAS of the registrations at the higher floors (roof and 11th floor).

In Figs. 10, 11 and 12 (Fig. 10: BI-2015-2, Table 1; Fig. 11: IS-2015-1, Table 2; Fig. 12: MC-1993-2, Table 3), the deconvolved wave fields using the recordings at the top of the buildings as reference and the corresponding spectra are shown for the same three

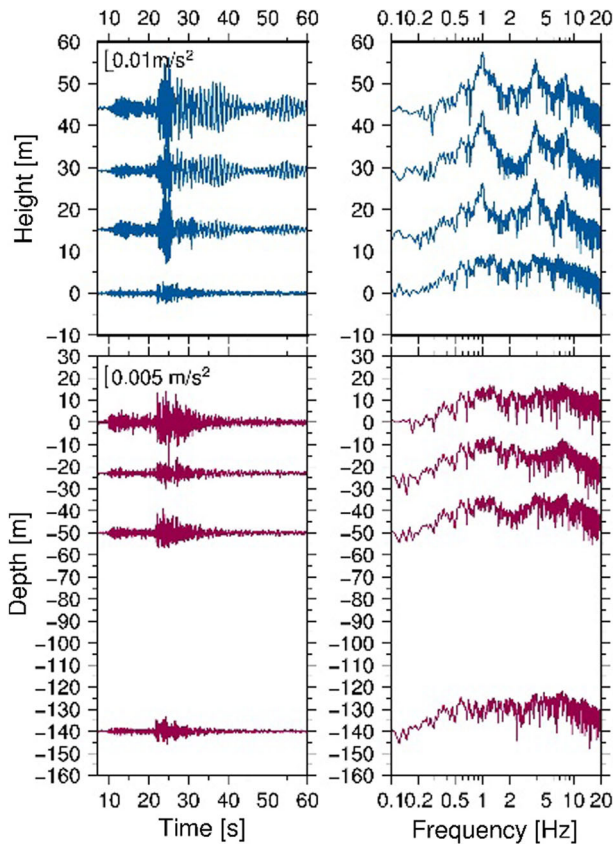


Fig. 8 Same as Fig. 7 but for the Istanbul vertical array, x-component, event IS-2015-1, Table 2

events as in Figs. 7, 8 and 9 for the three test cases (blue lines: building sensors, magenta lines: downhole sensors). For all three test cases, the up and downward propagating waves can be identified through the building-soil layers in the acausal and causal parts, respectively. When comparing the deconvolved wave fields for the three test cases, it is noticed that the deconvolved wave field of the Istanbul test site is dominated by more peaks, resulting in a more complex deconvolved wave field compared to the other two cases. Moreover, for the Mexico City test case, due to the narrow range of the frequencies for the building and soil, the peaks of the deconvolved wave field are wider. The transfer functions in the frequency domain show troughs associated with up and downward propagating waves for all three test cases. For the Istanbul test site, the transfer function of the downhole sensors and the building sensor at 0 m show troughs at the frequencies of the first two bending modes of the B22 building.

5.2 Estimation of the energy being radiated back from the building to the soil

The deconvolved wave fields are stacked for one horizontal component (Bishkek: transverse component, Istanbul: x-direction, see Fig. 5a, b) for all events for the test sites in Bishkek and Istanbul and are shown in Fig. 13a, b, respectively. Since the buildings have

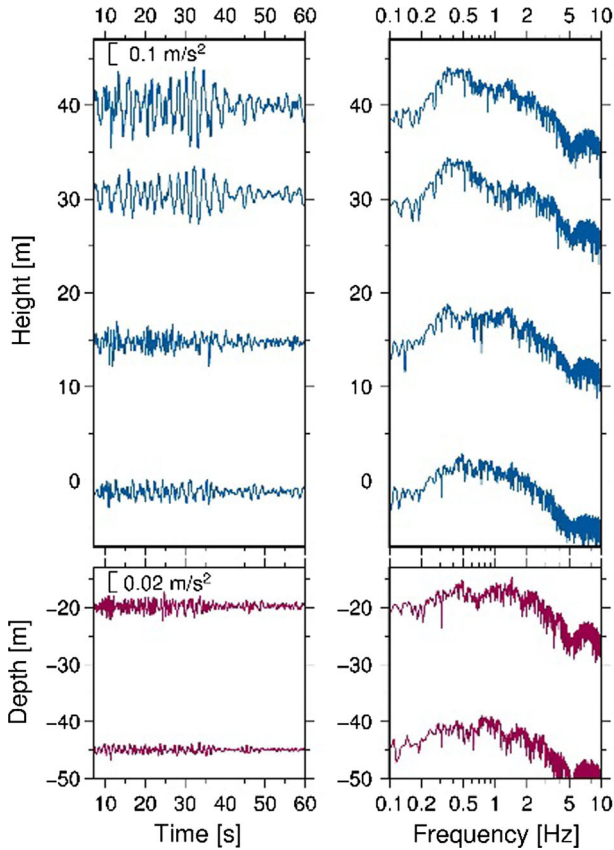


Fig. 9 Same as Fig. 7 but for the Mexico City vertical array, transverse component, event MC-1993-2, Table 3

not suffered any damage until now, the dynamic characteristics can be assumed to be constant, and thus, the results are stacked. Please note that the new dense installation of SOSEWINs in Istanbul was finalized in September 2015 and hence, for three earthquakes only the recordings at the top and bottom of the building are available. Moreover, the downhole sensor at 50 m depth suffered some malfunctions in November 2013, hence the recording of the two 2013 events are missing for this sensor. The dynamic characteristics of the Jalapa building in Mexico City have changed during the considered time period. Between the 1993 earthquakes and the events in 1997–1998, the Jalapa was damaged by a M_w 6.5 earthquake in 1994 and a M_w 7.5 earthquake in 1995, and was retrofitted in 1996–1997. For this reason, the results of the deconvolved wave fields are stacked for different time periods in which the structure is assumed to have the same dynamic behavior. The results are shown in Fig. 14a (1993 events after stacking), 14b (1997–1998 events after stacking) and 14c (MC-1999-2 event). The comparison of the deconvolved wave fields for the first two time periods (Fig. 14a, b) shows the change in the dynamic characteristics of the Jalapa building, i.e., the increase in the shear wave propagation velocity and, hence, the fundamental frequency in the transverse direction. After the 1998 event, another M_w 6.9 event occurred before the MC-1999-2 earthquake (Table 3), which

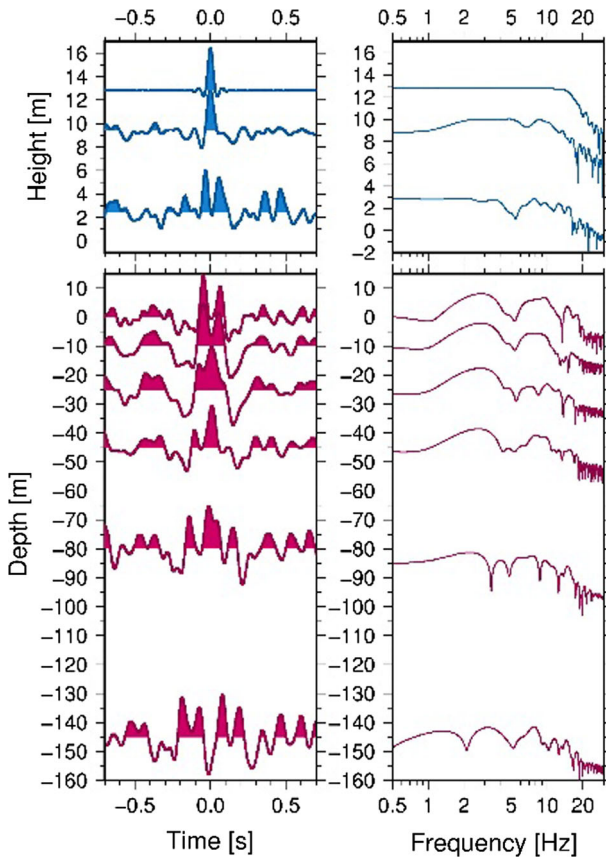


Fig. 10 Deconvolved wave fields using the recordings at the top of the building as the reference and the corresponding spectra of deconvolved wave fields for same events as for Fig. 7 for the building-downhole installation (blue lines building sensors, magenta lines downhole sensors) in Bishkek, event BI-2015-2, Table 1

caused structural damage, leading to a decrease in the shear wave velocity and the fundamental frequency.

For the three test cases, the different up and down-going waves contributing to the wave fields are marked by lines (e.g., Trampert et al. 1993) of different colors. The upward propagating waves can be identified at the deepest sensors (first peak in the acausal part marked by the first orange line), they propagate through the soil up to either the first impedance contrast or to the Earth's surface where a part of the energy is radiated back into the soil (black lines). The other part of the wave field is transmitted either to the adjacent soil layer or into the building layer. The remaining part propagates through the building up to the building's top (orange lines) where the wave field is reflected and propagates back down to the Earth's surface (green lines). When reaching the Earth's surface, one part of the wave field is reflected back into the building, whereas the other part is transmitted into the soil (green lines). This later part of the wave field is the one of major interest in this study. For the test cases in Bishkek and Mexico City, the downward propagating waves can be clearly identified down to the deepest sensor (Bishkek: at -145 m, Mexico City: at

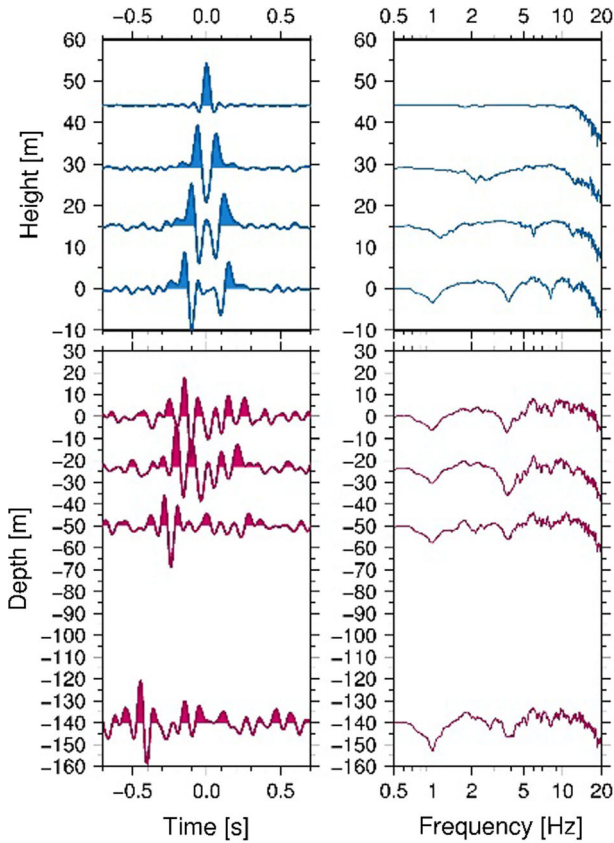


Fig. 11 Same as Fig. 10 but for the Istanbul vertical array for event IS-2015-1, Table 2

–45 m). For the test site in Istanbul, the peak associated with the downward propagating waves being radiated back from the building to the soil can be identified univocally in the deconvolved wave field down to 50 m depth.

Differently from the simple case where the sensors are installed in a homogenous layer and hence one upward and one downward propagating wave is obtained in the deconvolved wave field, for all three test cases, the structure of the building-soil-layer is more complex, as is the resulting deconvolved wave field. In order to better understand the wave propagation in the building-soil system and hence, the more complex deconvolved wave field, numerical simulations (comparisons of deconvolved wave fields of real and synthetic data) and the estimation of the analytical Transfer functions have been carried out.

The numerical simulations for the building-soil structure were performed using the Wang (1999) approach, based on a matrix propagator method which is stabilized numerically by inserting an additional numerical procedure into the matrix propagation loop. The simulations are carried out using sampling rates and generate a signal frequency band similar to that used with the real data. For this purpose, the buildings were assumed to behave as a shear beam and an additional layer for the building was added on the top of the soil layers. It is worth mentioning that assuming a building behaves as a pure shear beam is a very simplified model. Most buildings, such as for example the B22 building, do not

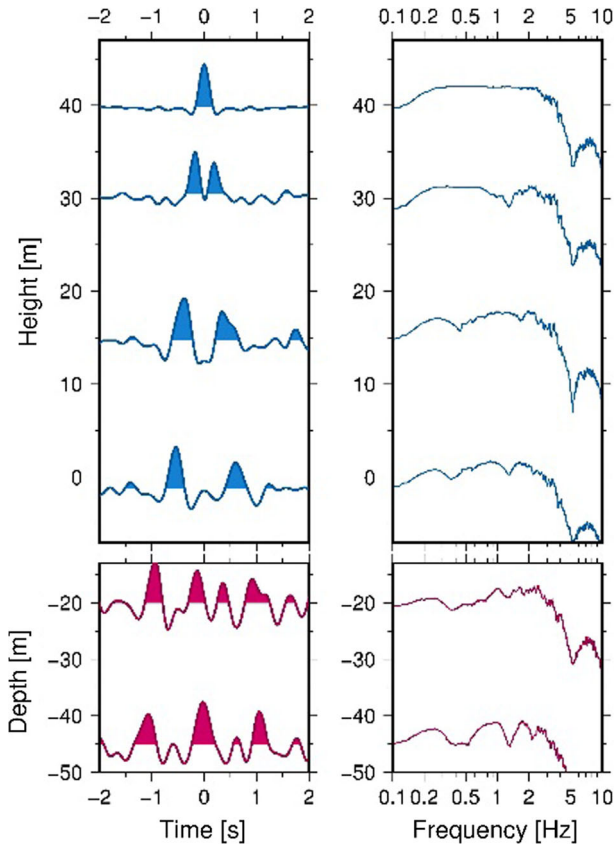


Fig. 12 Same as Fig. 10 but for Mexico City vertical array, event MC-1993-2, Table 3

behave as a pure shear beam, but as a combination of a shear and a bending beam (Petrovic et al. 2017). The scope of this study is not to find the model which describes the building's dynamic behavior in the best way, but, to model the building-soil structure in a simple way to make the interpretation of the real data results more easy. The correct positions of the peaks in time (defined by the velocity profile) and not the correct amplitude of the peaks (defined by the attenuation) are hereby of interest. For this reason, for the quality factor Q_s , an approximated value ($Q_s = 10$ for Bishkek and Istanbul and $Q_s = 20$ for Mexico City) is used. Studying the attenuation through the building-soil layers is beyond the scope of this study.

The deconvolution approach is also applied to the synthetic seismograms obtained by the numerical simulation. The deconvolved wave fields of the synthetic data (gray lines) are shown together with the results of the real data (blue lines: building sensors, magenta lines: downhole sensors) in Fig. 15 (a: Bishkek, b: Istanbul) and 16 (Mexico City, a: 1993 events after stacking, b: 1997–1998 events after stacking and c: MC-1999-2 event). For the test cases in Istanbul and Mexico City, two different simulations are used, namely the one including a building layer and the one without the building layer. It was observed that when considering only the model including the building layer (as for the case in Bishkek), the wave field reflected at the Earth's surface was not identified and the discrepancy

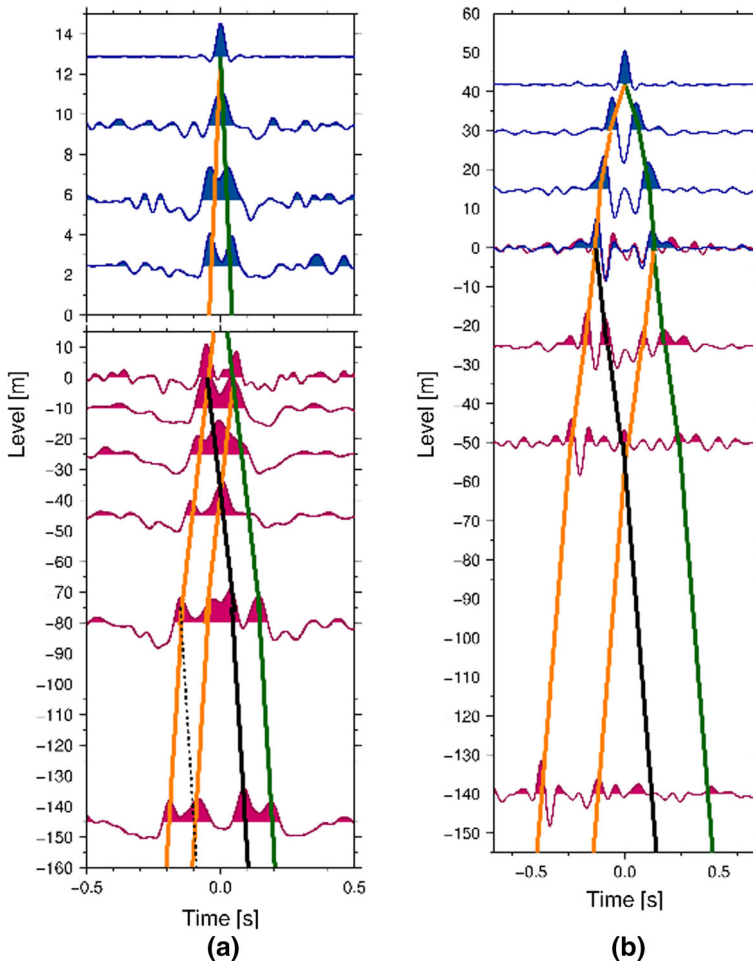


Fig. 13 Deconvolved wave fields (*blue lines* building sensor, *magenta lines* downhole sensors) obtained after stacking the results of all analyzed events for one horizontal component (*Bishkek* transverse direction; *Istanbul*: *x*-direction) using the recordings at the top of the building as reference. Orange, black and green lines correspond to upward propagating waves, downward propagating waves reflected at the Earth’s surface and the wave field radiated back from the building to the soil, respectively. **a** Bishkek VA, stacking of results of all events in Table 1; **b** Istanbul VA, stacking of results of all events in Table 2. Please note the *different vertical and horizontal scales* that are used for the different test sites

between the real and synthetic data results was large. Two aspects contribute to this discrepancy. On the one hand, the building is not a continuous layer and as for the Istanbul vertical array, the downhole installation is not below the building’s basement, but is shifted some tens of meters. Since there is no building layer above the borehole, more energy is being reflected at the Earth’s surface. The second aspect that explains the Mexico City test case is the Fresnel zone. Reflections do not take place at a single point, but over an area. This area is larger than the building’s footprint, and hence for this case, energy is also being reflected at the Earth’s surface and recorded at the downhole sensors. The results of the synthetic data for both models are plotted one above the other in Figs. 15b and 16.

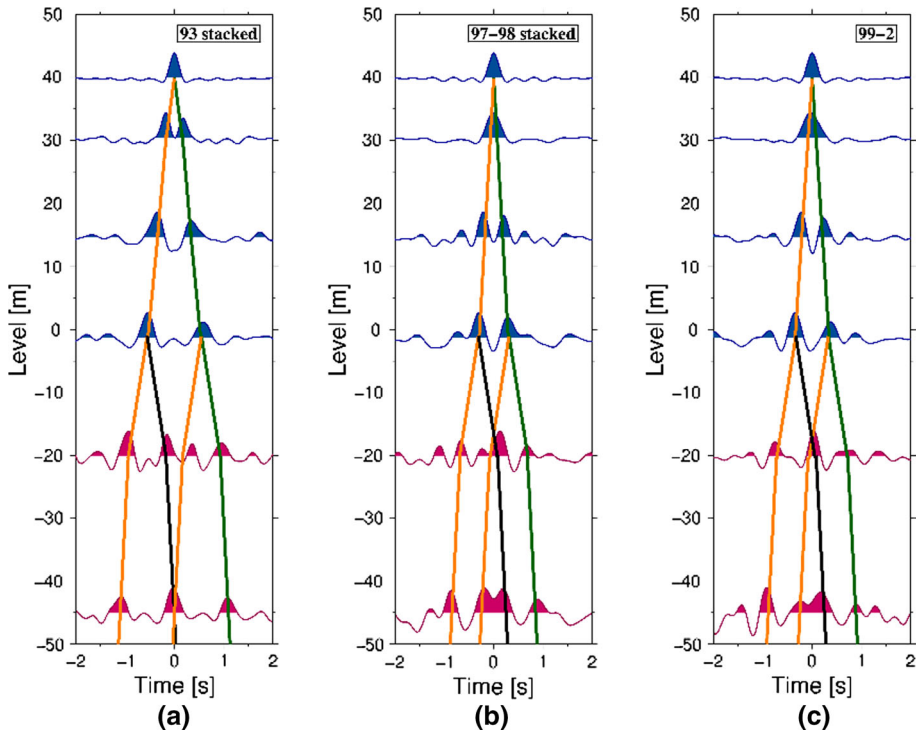


Fig. 14 Deconvolved wave fields (*blue lines* building sensor, *magenta lines* downhole sensors) obtained after stacking the results of events of different time periods for the Mexico City vertical array (transverse direction) using the recordings at the top of the building as reference. *Orange, black and green lines* correspond to upward propagating waves, downward propagating waves reflected at the Earth's surface and the wave field radiated back from the building to the soil, respectively. **a** Events of 1993, **b** events of 1997–1998, **c** event of 1999, Table 3

When comparing the results of the real and synthetic data, the similarity between the results for all three test cases is clearly visible. For the Bishkek test case, simply a better separation of the single peaks in the results of the synthetic data (probably due to different frequency bandwidths used for the analyses) and a discrepancy in the propagation velocities between -145 and -85 m can be observed. For the Istanbul test site, it can be seen that the deconvolved wave field of the real data set is dominated by peaks with inverted polarity that propagate from the building down to the soil with the same velocity and which are not observed in the results of the synthetic data set. As analyzed and discussed in detail in Petrovic et al. (2017), these peaks with inverted polarity are due to the excitation of the second bending mode and are projected to downhole sensors, since the recordings at the top of the building are used as the reference. Note that, in this case, modeling the building as an additional layer is a too simple model and hence, the contribution of the second bending mode cannot be seen in the results of the synthetic data. For the Mexico City test case, the agreement between synthetic and real data is very good, showing that the simplified model of building layers is sufficient in this case.

For the Bishkek test case, when considering the building and the soil layer above 75 m depth, the building-soil system can be modeled by two layers, while for sensors installed below 75 m depth a three-layer model is assumed. In Istanbul, when considering the soil

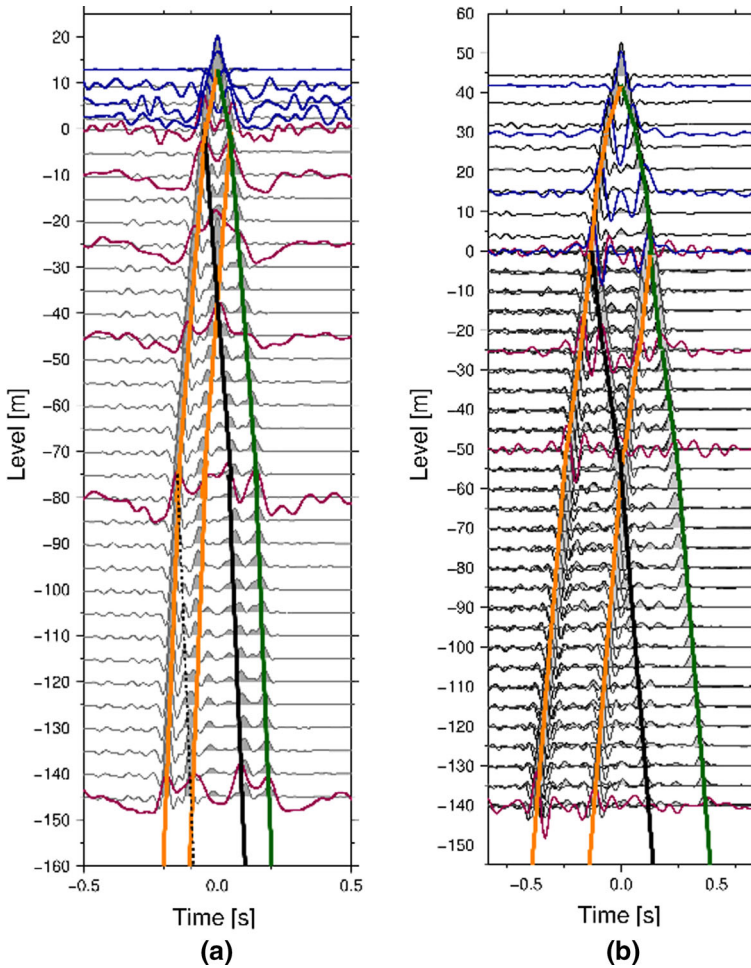


Fig. 15 Comparison of the deconvolved wave fields (*blue lines* building sensor, *magenta lines* downhole sensors) derived from real data obtained after stacking the results of all events (as shown in Fig. 13) and the synthetic data (*gray lines*) obtained from numerical simulations. *Orange, black and green lines* correspond to upward propagating waves, downward propagating waves reflected at the Earth's surface and the wave field radiated back from the building to the soil, respectively. **a** Bishkek VA; **b** Istanbul VA. Please note the *different vertical and horizontal scales* that are used for the different test sites

down to 50 m depth, a two layer system (one for the building and one for the soil) is used. For Mexico City, we examined one building layer for the Jalapa building and two soil layers (0–20 and 20–45 m).

The derivation of the analytical transfer functions for the sensor at the bottom of the downhole installation for both models (two and three-layer) can be found in the Appendix of Petrovic and Parolai (2016). When considering the two-layer model, the two peaks in the acausal part (orange lines in Figs. 13, 14, 15, 16) can be explained as follows: the first one is related to the upward going wave, while the second one must be taken into account when the recordings at the roof (affected by multiple reflections in the building that have to

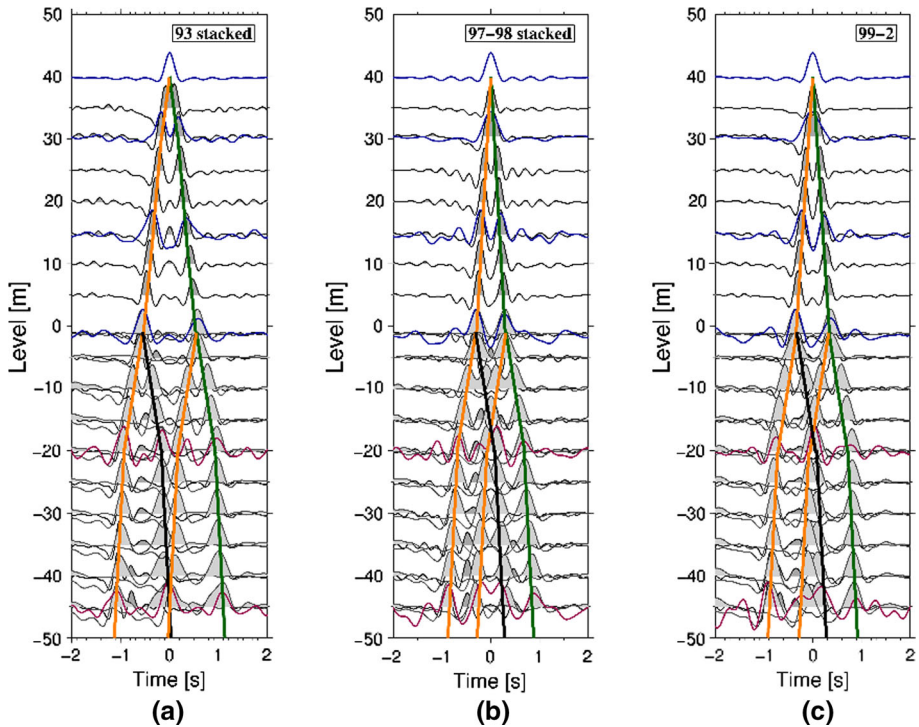


Fig. 16 Same as Fig. 15 but for the Mexico City vertical array. **a** Events of 1993, **b** events of 1997–1998, **c** event of 1999, Table 3

be removed) are back-projected to the borehole. To reconstruct the seismic input correctly, both peaks have to be considered.

The peak related to the part of the wave field that is radiated back from the building to the soil (green lines) overlaps with another peak corresponding to a wave which arrives at the same time. It is related to the part of energy that is missing in the recordings on the top of the building since it was reflected back at the Earth's surface. In order to reconstruct correctly the wave field that is related to the part of ground motion that is radiated back from the building into the soil layers, the relative contributions of these two peaks have to be considered. This is obtained from the terms $0.5(1 - r)$ (back-radiated wave field) and $r^2/[2(1 + r)]$ (wave field missing in the roof's top registration), with r being the reflection coefficient.

After the identification of the phases, the seismic input and the part of the wave field being radiated back from the building to the soil are estimated by the constrained deconvolution for the three test cases. In Fig. 17, the spectra of the reconstructed seismic input (blue lines) at a certain depth and the separated wave field being radiated back from the building to the soil for two depths (red and green lines) are shown exemplarily for Bishkek and Istanbul, in each case for one earthquake (a: BI-2015-2, Table 1; b: IS-2015-1, Table 2) and for one earthquake in each of the three considered time periods for Mexico City (c: MC-1993-2, d: MC-1997-1, e: MC-1999-2, Table 3).

For the test sites in Bishkek and Istanbul, the spectra of the downward propagating waves are dominated by the peaks of the first (Bishkek, Fig. 17a) or the three first

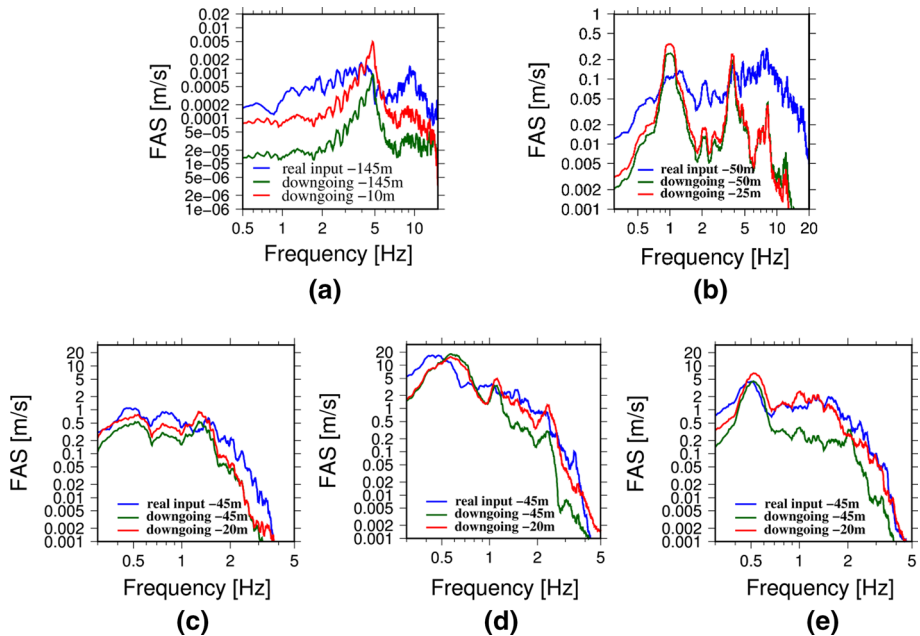


Fig. 17 **a** Bishkek: input spectrum at -145 m (blue), spectrum of down-going waves radiated back from the building reconstructed at -145 m (green) and at -10 m (red) for event BI-2015-2 (Table 1). **b** Istanbul: input spectrum at -50 m (blue), spectrum of down-going waves radiated back from the building at -50 m (green) and at -25 m (red) for event IS-2015-1 (Table 2). **c–e** Mexico City: input spectrum at -45 m (blue), spectrum of down-going waves radiated back from the building at -45 m (green) and at -20 m (red) for events MC-1993-2 (c), MC-1997-1 (d) and MC-1999-2 (e) (Table 3)

(Istanbul, Fig. 17b) bending modes in the considered direction. For Mexico City, the spectra of the reconstructed downward propagating waves show two peaks at the frequencies of the first two bending modes in this direction for the shown earthquake before the retrofitting (Fig. 17c), whereas the two events after the retrofitting show additionally also a peak at the frequency corresponding to the first torsional mode. Moreover, due to the fact that the dominant frequencies of the soil and the transverse direction of the building are very close (e.g., Meli et al. 1998), the peak of the first bending mode in the transverse direction and the resonance frequency of the soil (shown in the seismic input) are very close.

The velocity spectra of the seismic input and the wave field radiated back from the building to the soil are integrated (Bishkek: over a frequency range of $f = 1\text{--}10$ Hz, Istanbul $f = 0.1\text{--}15$ Hz, Mexico City: $f = 0.1\text{--}5$ Hz) in order to estimate the spectral energy. The selection of the frequency band was based on that of the spectra of the recording at the roof and is the same as the one used for the joint deconvolution. For the Bishkek vertical array, the energy that was radiated back by the building down to -145 and -10 m corresponds to 10 and 40–50% (the range corresponds to different events which were analyzed), respectively, of the energy of the seismic input at 145 m depth. At 145 m depth, there is almost no variation of the estimated spectral energy for different events, thus, only one value is given. For Istanbul, the energy associated with the downward propagating wave field at 25 and 50 m depth is estimated to be around 10–15% of the energy of the reconstructed seismic input at 50 m depth for both levels for the analyzed events. For Mexico City, the energy belonging to

the wave field radiated back from the building to the soil is estimated as 70–90% (at –20 m) and 25–65% (at –45 m) of the reconstructed seismic input at 45 m depth.

6 Discussion and conclusion

In this study, the analysis of wave propagation through three different building-soil structures was performed by the application of the joint deconvolution (Petrovic and Parolai 2016). The three different test cases consider different building construction types and shear wave velocity profiles of the buildings and underlying soil (and impedance contrasts between the buildings and the uppermost soil layer). The wave field associated with the seismic input (after removing the downward propagating waves) and the one associated with the wave field being radiated back from the building to the soil is separated by the constrained deconvolution approach. Finally, for all three test cases, the energy being radiated from the building back to the soil was estimated, concluding that the energy being radiated back is not negligible and possible interactions between buildings located close to each other should be taken into account.

Interestingly, when considering the spectra of the reconstructed downward propagating waves, these spectra are dominated by peaks at the fundamental frequencies of the buildings in all three test cases. For the Bishkek vertical array, a clear peak is observed at 5 Hz (corresponding to the first bending mode in the transverse direction). The spectra of the reconstructed down going waves for the Istanbul vertical array are dominated by three peaks at frequencies corresponding to the first three bending modes in the x-direction ($f_1 = 1$ Hz, $f_2 = 3.84$ Hz, $f_3 = 7.5$ Hz). For the Mexico City test site, the spectra of the downward propagating waves are dominated by different peaks before and after retrofitting. For the considered event before the retrofitting, the spectra show peaks at frequencies corresponding to the first two bending modes ($f_1 = 0.5$ Hz and $f_2 = 1.3$ Hz). After the retrofitting, the spectra show not only peaks at frequencies corresponding to the first two bending modes (MC-1997-1: $f_1 = 0.6$ Hz, $f_2 = 2.4$ Hz; MC-1999-2: $f_1 = 0.5$ Hz, $f_2 = 2.0$ Hz) but also a peak at a frequency corresponding to the first torsional mode (MC-1997-1: $f = 1.2$ Hz, MC-1999-2: $f = 1.1$ Hz).

For the Bishkek and the Istanbul test cases, the variation between the events of the amount of energy being radiated back from the buildings to the soil compared to the seismic input energy is very small for different events that have been analyzed. This is probably due to the fact that only weak motion events of a similar magnitude range and epicentral distance have been considered. For Mexico City, there is a larger variation of the energy being radiated back from the building to the soil compared to the seismic input energy for different events. This is consistent with the fact that the range of magnitudes and epicentral distances vary more for this test case and the dynamic properties of the building have changed due to damage and retrofitting over the different period considered. Analyzing the interactions of a building in which changes in the building construction have been performed, i.e., retrofitting, is similar to analyzing different buildings. For the Istanbul test site, the energy being radiated back from the building to the soil compared to the seismic input energy is the same (10–15%) for both considered depths. This is probably due to the fact that there is no impedance contrast between the two sensors installed at 25 and 50 m depths. For the test cases in Bishkek and Mexico City, the shear wave velocity increases with depth for the considered sensors and hence, the amount of energy being radiated back decreases.

The proportion of the observed wave field being radiated back from the building to the soil correlates inversely with the impedance contrasts. The Jalapa building has been damaged and retrofitted between the events in 1993 and 1997, leading to an increase of both the shear wave velocity through the building (from 70 to 140 m/s) and the effective density. Thus, the impedance contrast has decreased (from 0.3 to 0.6) followed by an increase of the amount of energy being radiated back from $\sim 45\%$ (MC-1993-1, MC-1993-2) to 55–65% (MC-1997-1, MC-1997-2 and MC-1998). The test cases in Bishkek and Istanbul have a higher impedance contrast compared to the Mexico City test case, less energy is being radiated back in this case. However, it is worth mentioning that different from Mexico City and Istanbul, for the Bishkek test case the energy being radiated back is considered at -145 m (at ~ 50 m depth for the other test cases).

The energy being radiated back from the building to the soil compared to the seismic input energy is estimated to be largest for the Mexico City test case. This is consistent with previous studies, where the soil–structure effects of the Jalapa building, which is constructed on soft soil, have already been confirmed. Moreover, the installation in Mexico City is the only one where the downhole installation is located directly below the building.

As summarized in the introduction, studying soil–structure interactions and site-city soil effects has found increasing interest over the last decades, especially when considering the use of 2D and 3D numerical simulations. Analyzing earthquake recordings from buildings and downhole installations provides the opportunity to learn about such interactions from real data and to better understand the ongoing processes, including wave propagation through building–soil layers. In this study, it was shown that downhole recordings are rich in information that on the one hand put questions on the standard uses, but on the other hand highlight the active role of built structures in shaping the wave field. Moreover, the obtained results suggest that a full comprehension of the wave field in the borehole recordings is necessary for improving studies of non-linearity in structures.

The interactions between the buildings and soil could not be identified in detail in these experiments and, therefore, more complicated 3D vertical arrays (multiple borehole–building network installations) are necessary. These installations would make it possible, first, to understand how the interactions are occurring, and second, to try to guide these interactions in order to minimize the effect of the input ground motion on the structures. Moreover, extensions to studies of building–building-interactions and site-city effects are required.

Acknowledgements The authors would like to thank Tobias Boxberger, Dino Bindi, Marco Pilz and Stefan Mikulla for the installation of the Self-Organizing Seismic Early Warning Information Network (SOSE-WIN) in the CAIAG Institute in Bishkek, and in the B22 building in Istanbul. The authors thank Messrs. Ahmet Korkmaz and Nafiz Kafadar of KOERI, Istanbul, for their efforts in maintaining the permanent installation at the B22 building. Moreover, we thank Vila-Murià for taking care of the Jalapa network and for sharing the data set (events from 1996 onwards) with us. This research was supported by the Global Change Observatory Central Asia and the Plate Boundary Observatory Turkey of the GFZ, and the MARsite project. Kevin Fleming kindly revised our English. Funding was provided by Cordis (MARsite, Project ID: 308417).

References

- Bard PY, Gueguen G, Wirgin A (1996) A note on the seismic Wavefield radiated from large building structures into soft soils. In: 11th world conference on earthquake engineering
- Bard PY, Chazelas JL, Gueguen P, Kham M, Semblat JF (2008) Site-city interaction. Assessing and managing earthquake risk. Springer, Berlin, pp 91–114

- Bertero M, Boccacci P (1998) Introduction to inverse problems in imaging. IOP Publishing, Bristol
- Bindi D, Parolai S, Picozzi M, Ansal A (2010) Seismic input motion determined from a surface-downhole pair of sensors: a constrained deconvolution approach. *Bull Seism Soc Am* 100:1375–1380
- Bindi D, Petrovic B, Karapetrou S, Manakou M, Boxberger T, Raptakis D, Pitilakis KD, Parolai S (2015) Seismic response of an 8-story RC-building from ambient vibration analysis. *Bull Earthq Eng* 13(7):2095–2120
- Boutin C, Roussillon P (2004) Assessment of the urbanization effect on seismic response. *Bull Seismol Soc Am* 94:251–268
- Cardenas M, Bard PY, Gueguen P, Chavez-Garcia FJ (2000) Soil–structure interaction in Mexico City. Wave field radiated away from Jalapa Building: data and modelling. In: 12th world conference on earthquake engineering; Auckland, New Zealand, Jan 30–Feb 4, 2000
- Cardenas-Soto M, Chavez-Garcia FJ (2007) Aplicación de la interferometría sísmica para obtener la respuesta de edificios y depósitos de suelo ante movimientos Fuertes. XVI Congreso Nacional de Ingeniería Sísmica, Ixtapa-Zihuatanejo (in Spanish)
- Céspedes I, Huang Y, Ophir J, Spratt S (1995) Methods for estimation of subsample time delays of digitized echo signals. *Ultrason Imaging* 17:142–171
- Chavez-Garcia FJ, Cardenas-Soto M (2002) The contribution of the built environment to the free-field ground motion in Mexico City. *Soil Dyn Earthq Eng* 22:773–780
- Chazelas JL, Abraham O, Semblat JF (2001) Identification of different seismic waves generated by foundation vibration: centrifuge experiments, time-frequency analysis and numerical investigations. In: 4th international conference on recent advances in geotechnical earthquake Engineering. And Soil Dynamics, San Diego
- Cheng MH, Kohler MD, Heaton TH (2015) Prediction of wave propagation in buildings using data from a single seismometer. *Bull Seism Soc Am* 105:107–119
- Colombi A, Roux P, Guenneau S, Gueguen P, Craster RV (2016) Forests as a natural seismic metamaterial: Rayleigh wave bandgaps induced by local resonances. *Sci Rep* 6:19238
- Ditommaso R, Mucciarelli M, Gallipoli MR, Ponzio FC (2009) Effect of a single vibrating building on free-field ground motion: numerical and experimental evidences. *Bull Earthq Eng* 8:693–703
- Faccioli E, Paolucci R, Vanini M (1996) Studies of site response and soil–structure interaction effects in a tall building in Mexico City. In: 11th world conference on earthquake engineering, Acapulco, Mexico, 23–28 June 1996
- Fleming K, Picozzi M, Milkereit C, Kühnlenz F, Lichtblau B, Fischer J, Zulfikar C, Özel O, SAFER and EDIM working groups (2009) The self-organizing Seismic early warning information network (SOSEWIN). *Seismol Res Lett* 80:755–771
- Guéguen P, Colombi A (2016) Experimental and numerical evidence of the clustering effect of structures on their response during an earthquake: a case study of three identical towers in the city of Grenoble, France. *Bull Seismol Soc Am* 106:2855–2864
- Guéguen P, Bard PY, Oliveira CS (2000) Experimental and numerical analysis of soil motions caused by free vibrations of a building model. *Bull Seismol Soc Am* 90:1464–1479
- Guéguen P, Bard PY, Chávez-García FJ (2002) Site-City seismic interaction in Mexico City-like environments: an analytical study. *Bull Seismol Soc Am* 92:794–811
- Isbilloğlu Y, Tabora R, Bielak J (2015) Coupled Soil–structure interaction effects of building clusters during earthquakes. *Earthq Spectra* 31:463–500
- Jennings PC (1970) Distant motions from a building vibration test. *Bull Seismol Soc Am* 60:2037–2043
- Kanai K (1965) Some new problems of seismic vibrations of a structure. In: Proceedings of the 3rd world conference on earthquake engineering, Auckland and Wellington, New Zealand
- Kanamori H, Mori J, Anderson DL, Heaton TH (1991) Seismic excitation by the space shuttle Columbia. *Nature* 349:781–782
- Kham M, Semblat JF, Bard PY, Dangla P (2006) Seismic site-city interaction: main governing phenomena through simplified numerical models. *Bull Seism Soc Am* 96:1934–1951
- Kitada Y, Kinoshita M, Iguchi M, Fukuwa N (1999) Soil–structure interaction effect on an Npp reactor building. Activities of Nupec: achievements and the current status. In: Celebi M, Okawa I (eds) Proceedings of the UJNR workshop on soil–structure interaction, Menlo Park, California, 22–23 Sept, paper no. 18
- Mazzieri I, Stupazzini M, Guidotti R, Smerzini C (2013) SPEED-spectral elements in elastodynamics with discontinuous Galerkin: a non-conforming approach for 3D multi-scale problems. *Int J Numer Methods Eng* 95:991–1010
- Mehta K, Snieder R, Grazier V (2007a) Extraction of near-surface properties for a lossy layered medium using the propagator matrix. *Geophys J Int* 169:2171–2280

- Mehta K, Snieder R, Grazier V (2007b) Downhole receiver function: a case study. *Bull Seismol Soc Am* 97:1396–1403
- Meli R, Faccioli E, Murià-Vila D, Quaas R, Paolucci R (1998) A Study of site effects and seismic response of an instrumented building in Mexico City. *J Earthq Eng* 2:89–111
- Murià-Vila DM, Rodriguez G, Zapata A, Toro AM (2001) Seismic response of a twice-retrofitted building. *ISET J Earthq Technol* 38:67–92
- Murià-Vila DM, Taborda R, Zapata-Escobar A (2004) Soil–structure interaction effects in two instrumented tall buildings. In: 13th world conference on earthquake engineering, Vancouver, BC, Canada, 1–6 Aug 2004, paper no. 1911
- Nakata N, Snieder R (2014) Monitoring a building using deconvolution interferometry. II: ambient-vibration-analysis. *Bull Seismol Soc Am* 104:204–213
- Newton C, Snieder R (2012) Estimating intrinsic attenuation of a building using deconvolution interferometry and time reversal. *Bull Seismol Soc Am* 102:2200–2208
- Oth A, Parolai S, Bindi D (2011) Spectral analysis of K-NET and KiK-net data in Japan, part I: database compilation and peculiarities. *Bull Seismol Soc Am* 101:652–666
- Paolucci R (1993) Soil-structure interaction effects on an instrumented building in Mexico City. *Eur Earthq Eng* 7(3):895–908
- Parolai S, Ansal A, Kurtulus A, Strollo A, Wang R, Zschau J (2009) The Ataköy vertical array (Turkey): insights into seismic wave propagation in the shallow-most crustal layers by waveform. *Geophys J Int* 178:1649–1662
- Parolai S, Bindi D, Ansal A, Kurtulus A, Strollo A, Zschau J (2010) Determination of shallow S-wave attenuation by down-hole waveform deconvolution: a case study in Istanbul (Turkey). *Geophys J Int* 181:1147–1158
- Parolai S, Wang R, Bindi D (2012) Inversion of borehole weak motion records observed in Istanbul (Turkey). *Geophys J Int* 188:535–548
- Parolai S, Bindi D, Ullah S, Orunbaev S, Usupaev S, Moldobekov B, Echtler H (2013) The Bishkek vertical array (BIVA): acquiring strong motion data in Kyrgyzstan and first results. *J Seismol* 17:707–719
- Petrovic B, Parolai S (2016) Joint deconvolution of building and downhole strong-motion recordings: evidence for the seismic wavefield being radiated back into the shallow geological layers. *Bull Seismol Soc Am* 106:1720–1732
- Petrovic B, Dikmen SU, Parolai S (2017) A real data and numerical simulations-based approach for estimating the dynamic characteristics of a tunnel formwork building: preliminary results (submitted)
- Pianese G, Petrovic B, Parolai S, Paolucci R (2017). Non-linear seismic response estimation of buildings by a combined Stockwell transform and deconvolution interferometry approach (submitted)
- Picozzi M, Parolai S, Mucciarelli M, Milkereit C, Bindi D, Ditommaso R, Vona M, Gallipoli MR, Zschau J (2009) Interferometric analysis of strong ground motion for structural health monitoring: the example of the L’Aquila, Italy, seismic sequence of 2009. *Bull Seismol Soc Am* 101:635–651
- Rahmani M, Todorovska MI (2013) 1D system identification of buildings during earthquakes by seismic interferometry with waveform inversion of impulse responses—method and application to Millikan library. *Soil Dyn Earthq Eng* 47:157–174
- Raub C, Bohnhoff M, Petrovic B, Parolai S, Malin P, Yanik K, Kartal RF, Kilic T (2016) Seismic-wave propagation in shallow layers at the GONAF-Tuzla site, Istanbul, Turkey. *Bull Seismol Soc Am* 106(3):912–927
- Semblat JF, Kham M, Gueguen P, Bard PY, Duval AM (2002) Site-city interaction through modifications of site effects. In: 7th conference of earthquake engineering, 2002, Boston, United States
- Semblat JF, Kham M, Bard PY, Gueguen P (2004) Could “site-city interaction” modify site effects in urban areas? In: 13th world conference on earthquake engineering Vancouver, BC, Canada
- Semblat JF, Kham M, Bard PY (2008) Seismic wave propagation in alluvial basins and influence on site-city interaction. *Bull Seismol Soc Am* 86:2665–2678
- Snieder R, Safak E (2006) Extracting the building response using seismic interferometry: theory and application to the Millikan library in Pasadena, California. *Bull Seismol Soc Am* 96:586–598
- Sorensen MB, Oprsal I, Bonnefoy-Claudet S, Atakan K, Mai PM, Pulido N, Yalciner C (2006) Local site effects in Ataköy, Istanbul, Turkey, due to a future large earthquake in the Marmara Sea. *Geophys J Int* 167:1413–1424
- Stockwell RG, Mansinha L, Lowe RP (1996) Localization of the complex spectrum: the S transform. *IEEE Trans Signal Process* 44:998–1001
- Tamim NSM, Ghani F (2010) Techniques for optimization in time delay estimation from cross correlation function. *Int J Eng Technol* 10:69–75
- Tikhonov AN, Arsenin VY (1977) Solution of ill-posed problems. Wiston/Wiley, Washington

- Trampert J, Cara M, Frogneux M (1993) SH propagator matrix and Q_s estimates from borehole- and surface-recorded earthquake data. *Geophys J Int* 112:290–299
- Wang R (1999) A simple orthonormalization method for stable and efficient computation of Greens functions. *Bull Seismol Soc Am* 89:733–741
- Wirgin A, Bard BY (1996) Effects of building on the duration and amplitude of ground motion in Mexico City. *Bull Seismol Soc Am* 86:914–920